Modeling of the competition between shear yielding and crazing in glassy polymers

Estevez, R.; Tijssens, M.G.A.; van der Giessen, E.

Published in:
Journal of the Mechanics and Physics of Solids

DOI:
10.1016/S0022-5096(00)00016-8

Publication date:
2000

Pergamon

Journal of the Mechanics and Physics of Solids
48 (2000) 2585–2617

JOURNAL OF THE
MECHANICS AND
PHYSICS OF SOLIDS

www.elsevier.com/locate/jmps

Modeling of the competition between shear yielding and crazing in glassy polymers

R. Estevez [1], M.G.A. Tijssens, E. Van der Giessen *

Delft University of Technology, Koiter Institute, Mekelweg 2, 2628 CD Delft, The Netherlands

Received 9 July 1999; received in revised form 10 January 2000

Abstract

Fracture in amorphous glassy polymers involves two mechanisms of localized deformations: shear yielding and crazing. We here investigate the competition between these two mechanisms and its consequence on the material's fracture toughness. The mechanical response of the homogeneous glassy polymer is described by a constitutive law that accounts for its characteristic softening upon yielding and the subsequent progressive orientational strain hardening. The small scale yielding, boundary layer approach is adopted to model the local finite-deformation process in front of a mode I crack. The concept of cohesive surfaces is used to represent crazes and the traction-separation law incorporates craze initiation, widening and breakdown leading to the creation of a microcrack. Depending on the craze initiation sensitivity of the material, crazing nucleates at the crack tip during the elastic regime or ahead of the crack. As the crazes extend, plasticity develops until an unstable crack propagation takes place when craze fibrils start to break down. Thus, the critical width of a craze appears to be a key feature in the toughness of glassy polymers. Moreover, the opening rate of the craze governs the competition between shear yielding and brittle failure by crazing.

Keywords: A. Fracture; A. Crack tip plasticity; B. Polymeric material; B. Elastic–viscoplastic material

* Corresponding author. Tel.: +31 15 278 6500; fax: +31 15 278 2150.
E-mail address: evandergiessen@wbmt.tudelft.nl (E. Van der Giessen).
[1] Present address: GEMPPM, INSA de Lyon, 21 Av Albert Einstein, 69621 Villeurbanne Cedex, France.

0022-5096/00/$ - see front matter
PII: S0022-5096(00)00016-8

1. Introduction

Crazing and shear yielding are the two primary localized deformation mechanisms intrinsic to glassy polymers. Shear yielding is plastic deformation in the form of shear bands which is intimately tied to the material softening that is observed right after yield. Upon further deformation, the material hardens due to molecular orientation and this leads to multiplication and propagation of shear bands. Crazing is due to the nucleation of microvoids in regions of stress concentrations and primarily normal to the maximum principal stress. These voids do not coalesce to form cracks since highly stretched molecular chains, or fibrils, stabilize this process to create crazes. However, after further craze widening, fibrils break down and a microcrack is formed.

Both processes have to be avoided in a properly designed component made of glassy polymers. Therefore, many studies aiming at a description of shear yielding and crazing have been carried out since the 1970's (see, e.g., Kambour, 1973; Haward, 1973). When crazing is dominant, this mechanism is considered as a precursor to brittle failure of the material (Kambour, 1973). Unlike crazing, shear yielding is thought to precede ductile failure because fracture involves relatively large deformations (Haward, 1973). Practically, a 'yield stress' and a 'crazing stress' are used in simple engineering estimates in order to determine which of these mechanisms is dominant at the given stress state and temperature (Haward, 1973). Such an approach tacitly assumes that crazing and shear yielding are independent mechanisms.

Even though this simple approach is useful for the initial stages of design, the simple identification with brittle or ductile failure hides the complex interaction between the two mechanisms. Although unstable crack propagation in glassy polymers is preceded by crazing, the reverse is not fully true: crazing can occur subsequent to plastic deformation (Ishikawa et al., 1977; Ishikawa and Ogawa, 1981; Ishikawa and Takahashi, 1991) or exist stably in glassy polymer blends like HIPS or ABS (Bucknall, 1977). In particular, Ishikawa and Ogawa (1981) point out the influence of the strain rate and the temperature on ductile or brittle failure in glassy polymers. Brittle failure is favored when the strain rate increases or when the temperature decreases while ductile failure is favored for opposite trends.

Studies on fracture in glassy polymers have mainly focused on brittle failure by crazing (Kinloch and Young, 1983; Williams, 1984) and are based on the standard linear elastic framework. Williams (1984) used a modified Dugdale model to represent a craze at a crack tip and postulated that the crack propagates when a critical opening of this zone is reached, as observed experimentally (Williams, 1984; Döll, 1983). For slightly viscoelastic materials, the experimental craze shape and that calculated from a zone uniformly loaded at the crack tip are similar. Some features of the crack growth for creep loading are also captured by this analysis (Williams, 1984). However, this approach hides the entire crazing process of initiation, widening and breakdown which is responsible for crack creation. Also, this model cannot be used when shear yielding of the material occurs because of its effect on the stress distribution. Thus, this approach of fracture in glassy polymers leaves room for

improvement to include the crazing mechanical response and the shear yielding in the bulk.

Any more detailed modeling than that referred to above was hindered by the fact that appropriate constitutive models were lacking. A significant advance was made by the model for plastic deformation in glassy polymers developed by Boyce et al. (1988). Lai and Van der Giessen (1997) recently adopted this model for an analysis of the development of plasticity around a blunted mode I crack in glassy polymers. This study pointed out that, owing to the intrinsic softening and final orientational hardening, plasticity develops in a pattern of shear bands, distinctly different from the standard fields in strain hardening metals. In particular, the location of the hydrostatic stress concentration, related to the plastic constraint, is shifted from the crack tip into the bulk as the shear bands expand. Void nucleation being a precursor to crazing, the location of high hydrostatic stress is thought to favor craze initiation (Ishikawa and Ogawa, 1981).

In this paper, we extend on this work (Lai and Van der Giessen, 1997) by including a description of crazing that allows us to study the interaction between plasticity and crazing during crack growth. The crazing is described by means of the cohesive surface model developed by Tijssens et al. (2000).

Tensors are denoted by bold-face symbols, $\otimes$ is the tensor product and $\bullet$ the scalar product. For example, with respect to a Cartesian basis $\boldsymbol{e}_i$, $\boldsymbol{AB}=A_{ik}B_{kj}\boldsymbol{e}_i\otimes\boldsymbol{e}_j$, $\boldsymbol{A}\bullet\boldsymbol{B}=A_{ij}B_{ij}$ and $\boldsymbol{LB}=L_{ijkl}B_{kl}\boldsymbol{e}_i\otimes\boldsymbol{e}_j$, with summation implied over repeated Latin indices. The summation convention is *not* used for repeated Greek indices. A prime $()'$ identifies the deviatoric part of a second-order tensor, $\boldsymbol{I}$ is the second-order unit tensor and tr denotes the trace.

2. Constitutive law for glassy polymers

The constitutive equations used to model the large strain plastic behaviour of the glassy matrix is based on original ideas by Boyce et al. (1988) but with some modifications introduced later by Wu and Van der Giessen (1993). The actual form adopted here, along with a convenient numerical integration scheme, is given in Wu and Van der Giessen (1996). The reader is referred to these references and the review in Van der Giessen (1997).

The rate of deformation $\boldsymbol{D}$ is decomposed into an elastic and a plastic part, $\boldsymbol{D}^{\mathrm{e}}$ and $\boldsymbol{D}^{\mathrm{p}}$ respectively: $\boldsymbol{D}=\boldsymbol{D}^{\mathrm{e}}+\boldsymbol{D}^{\mathrm{p}}$. Before plasticity takes place, $\boldsymbol{D}^{\mathrm{p}}=\boldsymbol{0}$, most amorphous polymers show a nonlinear stress–strain response which is caused by small strain viscoelastic effects. As we are primarily concerned in this study in the effect of matrix plasticity, the viscoelastic part of the response is not expected to affect the results significantly and will therefore not be explicitly accounted for. Instead, we shall represent the entire pre-yield response by a linear elastic one. In view of these approximations, it suffices to take the elastic response to be expressed by means of the hypoelastic law

$$\overset{\nabla}{\boldsymbol{\sigma}}=\boldsymbol{L}_{\mathrm{e}}\boldsymbol{D}^{\mathrm{e}}, \tag{1}$$

with $\boldsymbol{L}_e$ the usual fourth-order isotropic elastic modulus tensor in terms of Young's modulus E and Poisson's ratio ν, i.e., in Cartesian components,

$$L_{ijkl}=\frac{E}{2(1+\nu)}[(\delta_{ik}\delta_{jl}+\delta_{il}\delta_{jk})+\frac{2\nu}{1-2\nu}\delta_{ij}\delta_{kl}]. \tag{2}$$

The plastic part of the strain rate is taken to be specified by the viscoplastic constitutive equation

$$\boldsymbol{D}^p=\frac{\dot{\gamma}^p}{\sqrt{2}\tau}\bar{\boldsymbol{\sigma}}', \text{ with } \tau=\sqrt{\frac{1}{2}\bar{\boldsymbol{\sigma}}'\cdot\bar{\boldsymbol{\sigma}}'} \tag{3}$$

being the equivalent shear stress and $\bar{\boldsymbol{\sigma}}'$ the deviatoric part of the driving stress. The driving stress itself is defined by $\bar{\boldsymbol{\sigma}}=\boldsymbol{\sigma}-\boldsymbol{b}$, where $\boldsymbol{b}$ is the back stress tensor due to orientation hardening. The equivalent plastic shear rate $\dot{\gamma}^p$ is taken according to Argon's (1973) expression

$$\dot{\gamma}^p=\dot{\gamma}_0 \exp\left[-\frac{As_0}{T}\left\{1-\left(\frac{\tau}{s_0}\right)^{5/6}\right\}\right]. \tag{4}$$

where $\dot{\gamma}_0$ and A are material parameters and T is the absolute temperature. Eq. (4) is modified in order to account for the pressure dependence and the effect of strain softening on plastic flow, by using $s+\alpha p$ instead of s_0, where α is the pressure sensitivity parameter and $-p=\frac{1}{3}\text{tr}\,\boldsymbol{\sigma}$ is the mean (or hydrostatic) stress. Initially, s is equal to s_0, but evolves with plastic straining through

$$\dot{s}=h(1-s/s_{ss})\dot{\gamma}^p. \tag{5}$$

The saturation value of s is s_{ss}, while the parameter h controls the rate of softening. Upon substitution of Eq. (3), the plastic dissipation rate per unit volume, $\dot{D}$ is found to be given by

$$\dot{D}=\bar{\boldsymbol{\sigma}}'\cdot\boldsymbol{D}^p=\sqrt{2}\tau\dot{\gamma}^p. \tag{6}$$

The associated temperature rise has been ignored in this study as we assume that the time scale for the deformation is much larger than the time scale for heat diffusion. Hence, the deformation can be considered to be isothermal.

The progressive hardening of a glassy polymer after yield is due to the deformation-induced molecular orientation along the plastic stretch direction and is incorporated through the back stress $\boldsymbol{b}$ in the driving stress τ (see Eq. (3)). The description of the strain hardening in amorphous polymers makes use of the analogy with the stretching of the cross-linked network in rubbers (cf. Boyce et al., 1988). Neglecting for this purpose the elastic strains, the constitutive equations for the back stress tensor $\boldsymbol{b}$ are formulated through a functional description of its principal components b_α on the unit principal directions $\boldsymbol{e}_\alpha^p$ of the left stretch tensor, in terms of the corresponding principal stretches λ_α i.e.

$$\boldsymbol{b}=\sum_{\alpha} b_\alpha(\boldsymbol{e}^{\mathrm{p}}_\alpha\otimes\boldsymbol{e}^{\mathrm{p}}_\alpha),\ b_\alpha=b_\alpha(\lambda_\beta).$$

Here, to avoid confusion, principal tensor components and the corresponding eigenvectors are denoted with greek indices, for which the summation convention is not implied. The constitutive model used here, was proposed by Wu and Van der Giessen (1993) on the basis of their description of the fully three-dimensional orientation distribution of molecular chains in a non-Gaussian network. They showed that their numerical computations for such a network can be captured very accurately by the following combination of the classical three-chain network description and the Arruda and Boyce (1993) eight-chain model:

$$b_\alpha=(1-\rho)b_\alpha^{3-\mathrm{ch}}+\rho b_\alpha^{8-\mathrm{ch}}, \tag{7}$$

with ρ being determined by the maximum plastic stretch $\bar{\lambda}=\max(\lambda_1,\lambda_2,\lambda_3)$ through to $\rho=0.85\bar{\lambda}/\sqrt{N}$. Here, N is a statistical network parameter, which gives the average number of links between entanglements (or cross-links in a rubber) and thus determines the limit stretch $\lambda_{\max}$ of a molecular chain as $\lambda_{\max}=\sqrt{N}$. The principal back stress components $b_\alpha^{3-\mathrm{ch}}$ and $b_\alpha^{8-\mathrm{ch}}$ are given by

$$b_\alpha^{3-\mathrm{ch}}=\frac{1}{3}C^{\mathrm{R}}\sqrt{N}\lambda_\alpha L^{-1}\left(\frac{\lambda_\alpha}{\sqrt{N}}\right), \tag{8}$$

$$b_\alpha^{8-\mathrm{ch}}=\frac{1}{3}C^{\mathrm{R}}\sqrt{N}\frac{\lambda_\alpha^2}{\lambda_{\mathrm{c}}}L^{-1}\left(\frac{\lambda_{\mathrm{c}}}{\sqrt{N}}\right);\ \lambda_{\mathrm{c}}^2=\frac{1}{3}\sum_{\beta=1}^{3}\lambda_\beta^2, \tag{9}$$

where L denotes the Langevin function defined as

$$L(\beta)=\coth\beta-1/\beta.$$

The material parameter C^{R} governs the initial hardening modulus in shear. When the value of either $\bar{\lambda}$ or λ_{c} approaches $\lambda_{\max}$, the hardening rate increases dramatically, thereby suppressing effectively all further plastic flow, and the network locks. Therefore, for monotonic loading conditions, when either λ_α or λ_{c} exceeds the value $0.99\lambda_{\max}$, the network is 'locked' and no further viscoplastic flow is allowed.

Fig. 1 gives an example of the predicted response according to the above model, and illustrates the key characteristics of the materials under consideration. The material parameters, summarized in Table 1, are representative of SAN and will be used also for the results to be presented in Section 5.

3. Cohesive zone model of crazing

Since early observations of crazing in glassy polymers forty years ago, many studies have been devoted to the analysis of the craze structure by TEM or SAXS techniques and have attempted to identify the physical mechanisms involved in this pro-

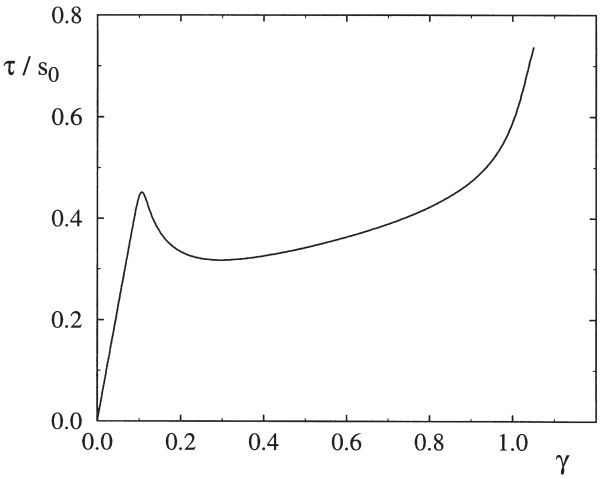

Fig. 1. Response of a glassy polymer (see Table 1) to simple shear.

Table 1
The set material parameters used in this study, representative of SAN at room temperature

	E/s_0	ν	s_{ss}/s_0	As_0/T	h/s_0	α	N	C^R/s_0
SAN	12.6	0.38	0.79	52.2	12.6	0.25	12.0	0.033

cess. An up-to-date account of these developments can be found in the reviews of Kambour (1973) and Kramer (1983) and of Kramer and Berger (1990). From a macroscopic point of view, crazes and cracks are geometrically similar: both appear as sharp planar surfaces. However, a craze is not a crack, but consists in fact of a web of interpenetrating voids and polymer fibrils. The fibrils are preferentially oriented in the direction normal to the craze plane, as illustrated in Fig. 2(a). The fibrils, comprising primary and secondary or cross-tie fibrils, bridge the craze surfaces so that load can be transmitted through the craze structure.

Crazing is generally thought to proceed in three stages (Kambour, 1973; Kramer, 1983): (i) initiation, (ii) widening, (iii) breakdown of the fibrils and creation of a crack. Unfortunately, the physical mechanisms involved in the various stages are still not clearly understood. As far as the mechanical behavior of crazes is concerned, different models have been proposed according to the length scale under consideration, as discussed in (Tijssens et al., 2000).

We choose to represent craze mechanical response using the concept of cohesive surfaces, due to Needleman (1987), as outlined in (Tijssens et al., 2000). The use of cohesive surfaces is quite intuitive from a morphological and mechanical point of view: experimental observations of crazes in glassy polymers (Kramer, 1983; Kramer and Berger, 1990) typically show a craze width of some microns and a length

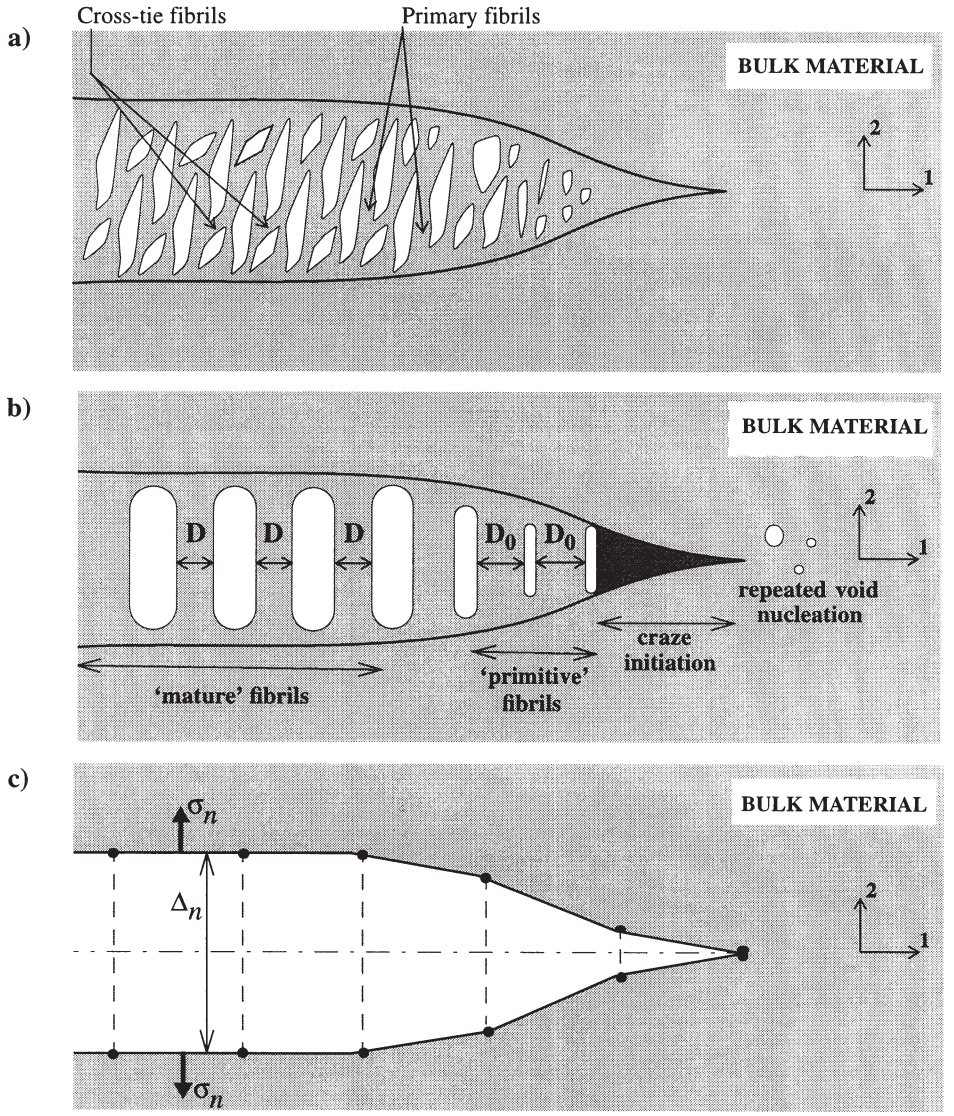

Fig. 2. Description of (a) the assumed craze structure, (b) the idealization of the craze structure according to the Kramer scheme (Kramer and Berger, 1990), representation of crazes by discrete cohesive surfaces.

of some decades larger, while further widening of the craze leads to the creation of a crack. By neglecting the actual fibrillar microstructure of a craze, these two observations motivate the use of a cohesive surface to describe a craze (see Fig. 2(c)), in which we distinguish three stages shown schematically in Fig. 2(b):

- prior to craze initiation, the two faces of the cohesive surface coincide and all fields are continuous across it;

- after initiation, the craze widens and the faces of the corresponding cohesive surface separate;
- the separation process ends with the creation of a crack, which is also represented by the cohesive surface but without load carrying capacity.

In the following, we present how we describe these three stages within the framework of cohesive surfaces. We conclude the section by the formulation of the traction-opening law which governs the constitutive response of a craze.

3.1. Craze initiation

Craze initiation and creation of a planar fibrillated structure from the bulk polymer are shown in Fig. 2(a). The physical mechanism for craze initiation has not yet been clearly identified and various criteria have been proposed according to the assumed mechanism and the length scale of its description. Experimentally one observes an incubation time for craze formation under constant applied stress and a saturation of the total craze nucleation sites (e.g., Kambour, 1973; Argon and Hannoosh, 1977). As the stress level increases, the incubation time decreases while the amount of craze sites at saturation increases, indicating that craze initiation is a stress dependent phenomenon.

Based on these experimental data and by borrowing some concepts from models of ductile failure in metals, Argon and Hannoosh (1977) have developed a rather sophisticated criterion for craze initiation. Craze formation is assumed to proceed as (i) nucleation of micro-voids and (ii) subsequent localized plastic drawing around these voids, leading to the (idealized) fibrillated structure in Fig. 2(b). These assumptions are partly confirmed by Argon and Salama (1977) who focus on the propagation of crazes from their nucleation sites. They show that for an applied tensile stress greater than 0.4–0.5 times the yield stress, craze propagation is well predicted by assuming a mechanism of repeated void nucleation. Furthermore, the incubation time for craze initiation at such a stress level is almost negligible since the material is ‘very rapidly’ (Argon and Salama, 1977) filled by craze initiation sites. For an applied tensile stress lower than 0.4–0.5 times the yield stress, an incubation time greater than 100 s is observed (Argon and Hannoosh, 1977). For such a level of stress, the ‘Taylor meniscus instability’ mechanism (Argon and Salama, 1977; Kramer, 1983) provides a better explanation of craze propagation.

We are concerned in this paper with the competition between shear yielding and crazing, so that we are naturally dealing with stress levels higher than 0.4–0.5 the yield stress. Motivated by the foregoing considerations we therefore neglect the incubation time for craze initiation and regard craze initiation to be an instantaneous process which arises when locally, a critical stress state is reached.

Based on similar assumptions for craze initiation, Sternstein and Ongchin (1969) propose a rather simple and empirical criterion. When compared to the Argon and Hannoosh (1977) formulation, both descriptions predict comparable critical stress states for crazing, except for stress states close to shear conditions (Tijssens et al., 2000). For the sake of simplicity, we choose to use the criterion formulated by

Sternstein and Ongchin (1969), but the framework is flexible enough to account for another criterion.

For plane stress conditions with σ_1 and σ_2 the principal stresses, Sternstein and Ongchin (1969) formulated a craze initiation criterion as

$$|\sigma_2-\sigma_1|\geq -A^0+\frac{B^0}{I_1},\ I_1>0. \tag{10}$$

where I_1 is the first stress invariant, $I_1=\sigma_1+\sigma_2$. The major principal stress direction defines the normal to the plane of the craze. The A^0 and B^0 in Eq. (10) are temperature dependent material parameters, which define a critical value for craze initiation under purely hydrostatic stresses through $I_1^{cr}=B^0/A^0$. The parameters A^0 and B^0 can be estimated from inhomogeneous stress–state experiments as carried out by Sternstein and Ongchin (1969) and Sternstein and Myers (1973).

Within the framework of the description of crazes with cohesive surfaces as in Fig. 2(c), we assume that the normal direction to the cohesive surface corresponds to the major principal stress, i.e. $\sigma_2\equiv\sigma_n$ in Eq. (10). If we further estimate the hydrostatic stress under conditions of plane strain in the 3-direction as $\sigma_m=\frac{1}{2}(\sigma_2+\sigma_1)$, the Sternstein criterion can be reformulated in terms of the normal traction σ_n as

$$\sigma_n\geq\sigma_m-\frac{A^0}{2}+\frac{B^0}{6\sigma_m}\equiv\sigma_n^{cr}(\sigma_m). \tag{11}$$

Since σ_2 is the major principal stress, we have $\sigma_n=\sigma_2\geq\sigma_m=\frac{1}{2}(\sigma_2+\sigma_1)$, so that the normal stress has to exceed the mean stress for craze initiation. According to Eq. (11), the criterion can be interpreted as a critical normal stress which is dependent on hydrostatic stress. Thus, crazing does not occur as long as $\sigma_n<\sigma_n^{cr}(\sigma_m)$ during a loading history; as soon as σ_n reaches $\sigma_n^{cr}(\sigma_m)$, crazing initiates. Once a craze has initiated, the craze widens and the condition Eq. (11) is no longer relevant.

3.2. Craze widening

Once a mature craze structure has been created, it widens by further fibrillation. Before powerful experimental techniques were available for craze microstructure observation, such as TEM (Lauterwasser and Kramer, 1979) or SAXS (Brown and Kramer, 1981), extension of the fibrils was thought to be by creep (e.g., Kambour, 1973). However, such a mechanism implies a variation of the fibril dimensions from the center of the craze towards its tip according to the increase of craze width. Careful TEM experiments (Donald and Kramer, 1981; Kramer, 1983; Kramer and Berger, 1990) have shown that fibrils have roughly a cylindrical shape and, in particular, that the craze volume fraction remains constant along the craze structure with ‘mature fibrils’ having an average diameter $D\approx$5–15 nm. At the craze tip, ‘primitive fibrils’ are estimated to have a diameter $D_0\approx$20–30 nm, depending on material (Kramer, 1983; Kramer and Berger, 1990). A creep mechanism appears to be in contradiction with these observations.

The currently accepted explanation is due to Kramer (1983) (see also, Kramer and

Berger, 1990) who has suggested that continued fibrillation occurs by a local drawing process of new polymers from an 'active zone' near the craze/bulk boundary into the fibrils, as illustrated in Fig. 3. He argues that chain disentanglement is involved during this process (Berger and Sauer, 1991) at the dome of the craze void along the so-called 'plane of separation' (see Fig. 3). Based on these postulates and assuming that the 'active zone' behaves as a non-Newtonian fluid they (Kramer, 1983; Kramer and Berger, 1990) arrive at a simple estimate for the widening rate.

A preliminary detailed finite element study of this process (Van der Giessen and Lai, 1997) using a more realistic material model is not fully consistent with the analysis of Kramer (1983) and Kramer and Berger (1990) and clearly more work is needed to clarify the process. By lack of a better description at this moment, we adopt here a phenomenological approach that is inspired by the results of Van der Giessen and Lai (1997). Since craze widening involves an intense viscoplastic activity in the active zone (see Fig. 3), this process has to be time and temperature dependent in a similar way to that of the homogeneous bulk polymer. We propose

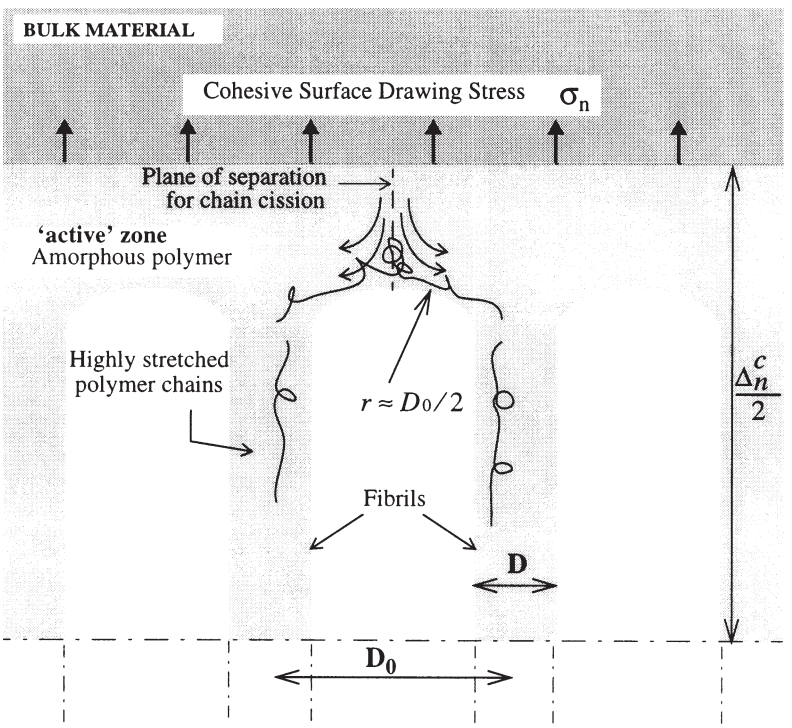

Fig. 3. Description of the craze widening process of Kramer (1983) as drawing in new polymer chains from the craze/bulk boundary into the fibrils.

to describe the craze widening process by a similar relation as the Argon expression Eq. (4), i.e.

$$\dot{\Delta}_n^c = \dot{\Delta}^0 \exp\left[\frac{-A^c\sigma^c}{T}\left(1-\frac{\sigma_n}{\sigma^c}\right)\right], \tag{12}$$

where $\dot{\Delta}_n^c$ represents the craze widening rate, and $\dot{\Delta}_0$, A^c and σ^c are material parameters; Δ_0 characterizes the time dependency of the craze widening process, σ^c represents the athermal stress for craze widening and A^c controls the temperature dependence.

3.3. Craze breakdown

The description of the final craze breakdown is still rather controversial in the polymer community and mainly two approaches have been developed.

Williams (1984) postulated that craze breakdown and subsequent crack propagation occurs when a critical craze opening displacement (COD), Δ^{cr}, is reached. From fracture experiments on various glassy polymers, (Döll, 1983; Döll and Könczöl, 1990) indeed observe such a critical constant craze maximum opening at the crack tip and during crack propagation, for different creep loadings. The experiments also show a craze length that is close to that predicted by Williams (1984). Nevertheless, Williams analysis assumes a viscoelastic response for the bulk and subsequent deformation of the crazes by creep. Such assumption implies that breakdown of the fibrils occurs most probably at the center, where the 'oldest' and more deformed fibrils are located. There are no experimental results, however, that confirm this.

On the contrary, Kramer and Berger (1990) reported that failure of fibrils in several glassy polymers initiates at the craze/bulk interface and not at the center of the craze width (Berger, 1990). They observe that the maximum craze width at breakdown is dependent on molecular weight due to the loss of entanglements during the craze widening process. Berger (1990) identified a critical molecular weight M_c and distinguishes three domains: (i) if $M_w<M_c$, no stable craze is observed; (ii) a transition regime where the craze stability is highly dependent of the material M_w while (iii) for higher M_w, a regime exists in which the maximum craze width is roughly constant.

Berger (1990) concluded that if craze stability is available, the craze widening process continues until the craze/bulk interface encounters a flaw sufficient for critical loss of entanglements and subsequent fibril breakdown. Kramer and Berger (1990) formulated a statistical description of craze failure to represent the probability of such an event to occur, depending on the craze width. Although their analysis has different foundations from that of Williams (1984), it also leads to a critical craze width Δ^{cr} before fibrils break down, Δ^{cr} being molecular weight dependent. Furthermore, if craze breakdown is related to the presence of microstructural defects or flaws in the material, then Δ^{cr} will also depend on the preparation process (quenched vs slow cooling, presence of plasticizers, etc.).

In the light of these observations and descriptions, we choose, as a first approximation, to describe craze breakdown within the cohesive surface framework by defining a similar critical craze width $\Delta_n^{c\,cr}$. After craze initiation and subsequent

widening, the parameter $\Delta_n^{c\,cr}$ represents a limit for the accumulated craze widening as governed by Eq. (12). When this limit is reached, the craze widening process ends and a microcrack is formed.

Of course such a simple rule hides much of the underlying physics, but this is not well understood at the moment. The criterion can obviously be improved. For example, Sha et al. (1997) and Hui et al. (1992) have recently demonstrated the importance of the cross-tie fibrils in the breakdown process. Evidently, this is a feature of the actual microstructure of a craze on a smaller scale than can be captured by a cohesive surface model. The cross-tie fibril effect is therefore considered here to be collapsed somehow in the value of $\Delta_n^{c\,cr}$.

3.4. Traction evolution law for the cohesive surfaces

The elemental processes of crazing described in the foregoing sections, Δ_n^c of the craze widening and Δ_n related to the cohesive surface opening, are completed by the traction-opening law

$$\dot{\sigma}_n = k_n(\dot{\Delta}_n - \dot{\Delta}_n^c) = k_n \dot{\Delta}_n^e \tag{13}$$

in which $\dot{\Delta}_n$ is the normal opening rate of the cohesive surface, $\dot{\Delta}_n^c$ is the widening rate of the craze according to Eq. (12) and $\dot{\Delta}_n - \dot{\Delta}_n^c$ represents the elastic contribution to the opening rate. k_n is an elastic stiffness which has to be specified. Prior to craze initiation, the cohesive surface stiffness k_n has to be such that the elastic widening remains 'infinitely' small so that the cohesive surface does not affect the fields. When craze widening takes place, k_n should represent the stiffness of the fibrillated structure.

Experimental observations in (Kramer, 1983; Kramer and Berger, 1990) show that the fibril diameter evolves from D_0 at the craze tip to a constant D along the craze (Fig. 2(b)). Donald and Kramer (1982) show that the diameter of the 'mature' fibrils D relative to the initial 'primitive' D_0 is correlated to the chain entanglement density. They suggest that in the early stage of craze widening, prior to the start of the drawing in mechanism described in Section 3.2, the 'primitive' fibrils are stretched to form 'mature' fibrils. By accounting for the cylindrical geometry of the fibrils and by assuming that this stretching occurs at constant volume, one finds that $D = D_0 \lambda^{-1/2}$, in which λ corresponds approximately to the maximum stretch λ_N of the polymer chain between two entanglements (Donald and Kramer, 1982). The initial length h of the 'primitive' fibrils D_0 at the craze tip ranges between 5 nm and D_0.

Based on these observations, we propose to define the cohesive surface stiffness k_n for the various stages of crazing as follows:

- Craze initiation corresponds to the creation of 'primitive' fibrils of diameter D_0 and length h, when the normal stress $\sigma_n = k_n^0 \Delta_n$ attains a critical value of σ_n^{cr} according to Eq. (11). By assuming that the opening $\Delta_n \equiv h$ at initiation, the initial stiffness of the craze is

$$k_n^0 = \frac{\sigma_n^{cr}}{h} \tag{14}$$

- While the void structure evolves to a structure of 'mature' fibrils, the diameter of the fibrils decreases according to $D=D_0\lambda^{-1/2}$ where λ is the stretch of the fibril. The latter can be estimated from the foregoing as $\lambda=\Delta_n/h$. Treating the fibril as a strut, for simplicity, we can define a fibril stress σ_f by $\sigma_f=(D_0/D)^2\sigma_n=\lambda\sigma_n$ which increases with λ during this process. If the elastic modulus of the material in the fibril remains constant, the overall stiffness of the fibril strut therefore scales with $1/\lambda$ and so does k_n, i.e.

$$k_n=\frac{k_n^0}{\lambda}. \tag{15}$$

- Once the 'mature' fibrils have formed, the current fibril material consists of highly stretched molecules. The overall instantaneous elastic stiffness of the craze, k_n, is therefore assumed to arise primarily from the freshly drawn-in fibril material. Hence, k_n is taken to be constant during drawing and equal to the limiting value k_n^0/λ_Naccording to Eq. (15).
- Prior to craze initiation, $\sigma_n<\sigma_n^{cr}(\sigma_m)$ in Eq. (11), the stiffness should be 'infinitely large' to ensure that no separation of the cohesive surfaces is observed for any value of the normal stress. For numerical convenience, we propose to define

$$k_n^{\infty}=\frac{\sigma_n^{cr}(\sigma_m)}{h}, \tag{16}$$

with σ_m the instantaneous hydrostatic stress. When the initiation criterion Eq. (11) is fulfilled, Eqs. (14) and (16) are identical. Thus, the cohesive stiffness decreases gradually. Practically, the value of k_n^{∞} is limited by a chosen arbitrarily high one, about ten times larger than that at initiation, k_n^0.

To conclude this section, Fig. 4 shows the full traction-opening response to a constant

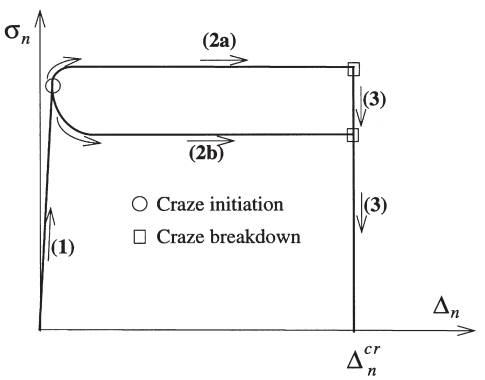

Fig. 4. Schematic representation of the cohesive surfaces traction-opening law: 1) no crazing, 2) craze widening [(a) hardening-like response, (b) softening response], 3) craze breakdown at $\Delta_n=\Delta_n^{cr}$ and subsequent crack formation.

opening rate $\dot{\Delta}_n$ obtained from Eq. (13). In accordance with the first three subsections, three regimes are distinguished:

1. as long as crazing has not yet initiated, the stress applied on the cohesive zone can increase without generating any significant opening;
2. after a short transition stage following initiation, the fibrillation process leads to a widening Δ_n of the cohesive surfaces at an approximately constant normal stress σ_n;
3. when the craze width reaches the critical value $\Delta_n^{c\,cr}$, it breaks down and a microcrack is formed with a corresponding vanishing of the traction.

Depending on the the difference between the cohesive surface opening rate $\dot{\Delta}_n$ and the craze opening rate $\dot{\Delta}_n^c$, the traction-opening response exhibits (a) a hardening-like or (b) a softening behaviour (see Fig. 4). In particular, for a given $\dot{\Delta}_n$, the response depends on the parameters $\dot{\Delta}^0$, A^c and σ^c from Eq. (12), which define the craze widening rate $\dot{\Delta}_n^c$. The competition between these two term defines which widening behaviour take place: (a) $\dot{\Delta}_n > \dot{\Delta}_n^c$, (b) $\dot{\Delta}_n < \dot{\Delta}_n^c$.

4. Numerical study

Lai and Van der Giessen (1997) performed a finite element study of the crack-tip plasticity and near-tip stress fields of a mode I crack in glassy polymers, without accounting for crazing. This work pointed out that, as a consequence of the plastic deformation pattern, the maximum hydrostatic stress distribution differs from the well-known HRR solution in plastically hardening materials. Due to the intrinsic softening followed by orientational hardening of these materials (see Fig. 1), shear bands initiate around the crack tip and intersect along the crack symmetry plane. Due to plastic incompatibility, the maximum hydrostatic stress is located at the shear band intersection. This location moves away from the crack tip into the bulk material as plasticity develops.

In the present paper we proceed from this study by accounting for possible crazing. Since craze initiation is hydrostatic stress dependent (Eqs. (10) and (11)), it is expected that crazing occurs preferentially along the crack symmetry plane. We therefore consider only a single cohesive surface along this plane, even though the framework allows us to embed cohesive surfaces throughout the volume as performed in (Tijssens et al., 2000).

Following Lai and Van der Giessen (1997), we consider an initially blunted crack with a finite root radius r_t. Plasticity and crazing are assumed to be confined around the crack tip so that the small scale yielding framework is allowed. The boundary layer approach is used to investigate the mode I plane strain fields near the crack. Traction-free boundary conditions are imposed along the crack face and a cohesive surface is laid out ahead of the crack along the symmetry plane. Because of the symmetry about the crack plane, only one half of the geometry needs to be analyzed

(see Fig. 5(a)). The remote region is taken to be bounded by a circular arc of radius R surrounding the crack tip of radius r_t with $R/r_t \approx 200$. Along this arc, the mode I elastic field at a stress intensity factor K_I is prescribed via the displacement components u_1 and u_2, in the Cartesian frame x_i, according to

$$u_1 = 2(1+\nu)\frac{K_I}{E}\sqrt{\frac{r}{2\pi}}\cos\frac{\theta}{2}\left[2-2\nu-\left(\cos\frac{\theta}{2}\right)^2\right], \tag{17}$$

$$u_2 = 2(1+\nu)\frac{K_I}{E}\sqrt{\frac{r}{2\pi}}\sin\frac{\theta}{2}\left[2-2\nu-\left(\cos\frac{\theta}{2}\right)^2\right], \tag{18}$$

where r and θ are polar coordinates with the origin located at the crack tip. Loading is prescribed to increase at a constant $\dot{K}_I$. Fig. 5(b) shows the finite element mesh in the remote and the crack tip regions.

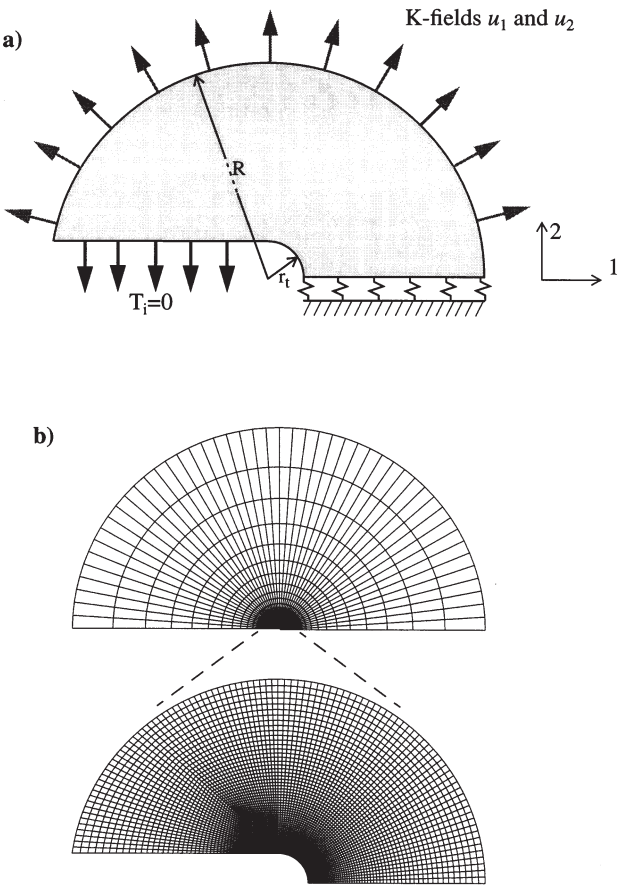

Fig. 5. Problem formulation and finite element mesh used in the analysis. (a) boundary conditions; (b) outer mesh and near crack tip mesh.

A quasi-static finite strain analysis is carried out, in which we use a total Lagrangian description of the continuum field equations while the cohesive surface is analyzed in its current configuration. Virtual work for this problem is then expressed as

$$\int_V \boldsymbol{\tau}\cdot\delta\dot{\boldsymbol{\eta}}\,dV+\int_{S_c}\sigma_n\delta\dot{\Delta}_n\,dS=\int_{\partial V}\boldsymbol{T}\cdot\delta\boldsymbol{v}\,dS, \tag{19}$$

with V and ∂V denoting the volume of the region in the initial configuration and its boundary, respectively, and with S_c denoting the cohesive surface in the current state. Furthermore in Eq. (19), $\boldsymbol{\tau}$ is the second Piola–Kirchhoff stress tensor, $\boldsymbol{T}$ the corresponding traction vector; $\dot{\boldsymbol{\eta}}$ and $\boldsymbol{\nu}$ are the conjugate Lagrangian strain rate and velocity. The governing equations are solved in a linear incremental fashion based on the rate form of Eq. (19), supplemented with an equilibrium correction. The stress and strain rates appearing in this rate form can be related in the standard way to the rate of Cauchy stress $\boldsymbol{\sigma}$ and the stretching rate $\boldsymbol{D}$ used for the constitutive description (Section 2). Details may be found in (Wu and Van der Giessen, 1996). After substitution of the constitutive Eq. (13) for the cohesize surface, one ultimately arrives at a set of equations that have the standard form for elasto–viscoplastic problems.

The equations are discretized using quadrilateral elements built up of four linear triangular elements in the bulk and linear line elements along the cohesive surface. Newton–Cotes integration is used to integrate the equations along the cohesive elements (Tijssens et al., 2000). The location of this latter being restricted to the symmetry axis, the hydrostatic stress involved in Eq. (11) is estimated from the mean value of σ_m of the continuum elements adjacent to the considered cohesive surface element.

In order to improve the numerical stability of the viscoplastic solution in the bulk amorphous polymer, a rate tangent formulation of the constitutive Eqs. (1)–(3) is used (Wu and Van der Giessen, 1996). For the constitutive equation for crazing, Eq. (13), we use a similar scheme on the basis of a forward gradient integration of the widening term Δ_n^c, as developed by Tijssens et al. (2000). This leads to the definition of a stiffness k_n^*,

$$k_n^*=k_n\left(1+k_n\theta\frac{\partial\dot{\Delta}_n^c}{\partial\sigma_n}\Delta t\right), \tag{20}$$

to be used during a time step Δt ($\theta\in[0,1]$). This stiffness is then used to replace Eq. (13) with the expression

$$\dot{\sigma}_n=k_n^*(\dot{\Delta}_n-\dot{\Delta}_n^c). \tag{21}$$

The integration scheme is further improved by calculation of the exact solution for

the normal traction increment $\Delta\sigma_n$ between t and $t+\Delta t$. From Eqs. (12) and (13), by invoking that $\dot{\Delta}_n^c$ is constant during Δt, one obtains

$$\Delta\sigma_n = -\frac{T}{A^c}\ln\left\{\left(1-\frac{\dot{\Delta}_0}{\dot{\Delta}_n}\exp\left[-\frac{A^c}{T}(\sigma^c-\sigma_n)\right]\right)\exp\left[-\frac{A^c}{T}k_n\dot{\Delta}_n\Delta t\right]+ \frac{\dot{\Delta}_0}{\dot{\Delta}_n}\exp\left[-\frac{A^c}{T}(\sigma^c-\sigma_n)\right]\right\}. \tag{22}$$

When craze breakdown occurs, the value of σ_n is decreased to zero within few increments to avoid numerical instabilities during the unloading regime 3 of Fig. 4.

Finally, it has been found necessary to employ an adaptive time step procedure both for the bulk viscoplastic solution (Wu and Van der Giessen, 1996) and for the cohesive surface model. In the latter, the time step is adapted to control the increments $\Delta\sigma_n$ and $\dot{\Delta}_n$ within each time step. The used margins are $\Delta\sigma_n < 10^{-2}\sigma^c$ and $\Delta t\dot{\Delta}_n < 10^{-2}\Delta_n^{c\,cr}$.

5. Results and discussion

A parameter study has been performed in order to identify the main parameters that drive the competition between shear yielding and crazing in glassy polymers. The set of material constants (see Table 1) chosen for the bulk material corresponds to that of SAN at room temperature (stress-like variables are non-dimensionalized with the athermal yield stress s_0=119.5 MPa) and the corresponding response is shown in Fig. 1. To get some insight in the influence of the various parameters in the craze model presented in Section 3, eight sets of craze parameters have been selected and listed in Table 2. The case number 1 in Table 2 is used as a reference case. These parameters do not refer to a particular material. The reference values of A^0, B^0, and $\Delta_n^{c\,cr}$ have been picked on the basis of experimental data (Sternstein and Ongchin, 1969; Döll, 1983) while the values of $\dot{\Delta}^0$, σ^c and A^c in the kinetic relation

Table 2
The sets of craze parameters used in this study

case	A^0/s_0	$B^0/(s_0)^2$	$\Delta_n^{c\,cr}/r_t$	σ^c/s_0	$A^c\sigma^c/T$	$\dot{\Delta}^0/r_t$ (sec^{-1})
1	0.68	1.4	0.1	0.83	44.1	100
2	0.68	2.8	0.1	0.83	44.1	100
3	0.68	1.4	0.01	0.83	44.1	100
4	0.68	1.4	0.2	0.83	44.1	100
5	0.68	1.4	0.1	0.83	44.1	10
6	0.68	1.4	0.1	0.83	44.1	1
7	0.68	1.4	0.1	0.83	44.1	0.1
8	0.68	1.4	0.1	0.83	136.5	100

Eq. (12) for craze widening have been chosen intuitively with reference to the bulk parameters in Table 1.

An applied loading rate of $\dot{K}_I^0 \approx 3.10^{-2}\text{MPa}\sqrt{\text{m}}/\text{sec}$ is taken as reference. For a crack root radius of r_t=0.1 mm, such a loading rate is consistent with a displacement rate on the order of 5×10^{-5} m/sec in the remote region of the specimen (about 20 mm from the crack tip). In the first two subsections, we investigate the effect of the craze initiation parameters A^0 and B^0 Eq. (11), and that of the maximum craze widening $\Delta_n^{c\,cr}$ (Section 3.3). In the subsequent subsections, the influence of the loading rate is explored through different values of $\dot{K}_I$. Special attention will be given then to the influence of craze widening kinetics governed by $\dot{\Delta}_0$ and A^c/σ^c. The influence of temperature on crazing has been briefly investigated by Tijssens et al. (2000) and is not considered in the present study.

5.1. Influence of the craze initiation parameters

According to Eq. (11), craze initiation is governed by two material parameters: A^0 and B^0. Two sets of craze parameters (cases number 1 and 2 in Table 2) are sufficient to get an understanding of their influence. The two differ only in the value of B^0. Fig. 6(a) shows the corresponding craze initiation loci in $\sigma_n-\sigma_m$ space. We observe that the criterion with the largest value of B^0 requires a higher stress state in terms of (σ_n,σ_m) for craze initiation. In either case, the actual initiation stress depends quite sensitively on the ratio σ_n/σ_m.

To get some insight in this ratio near a crack tip, we first analyze the opening

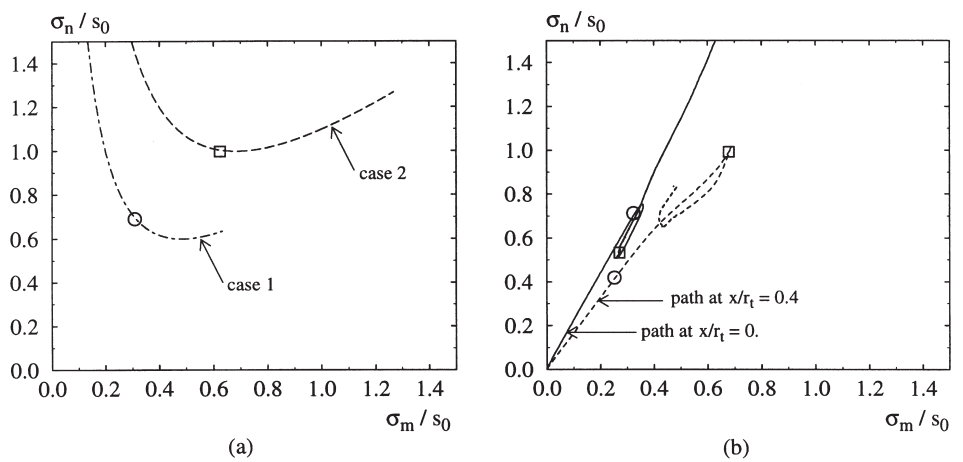

Fig. 6. Influence of the craze initiation parameter on the initiation location for: i) case 1, A^0/s_0=0.68 and B_0/s_0^2=1.4 ii) case 2, A^0/s_0=0.68 and B_0/s_0^2=2.8. (a) corresponding craze initiation condition, (b) evolution of (σ_n,σ_m) for the cohesive surface at x/r_t=0 and at x/r_t=0.4 if crazing would not intervene. The circles and the squares indicate the stress state in both location at first craze initiation according to cases 1 and 2, respectively.

crack without crazing. Then, the response of the cohesive surface is governed by $\dot{\sigma}_n = k_n^{\infty}\dot{\Delta}_n$ with a very large value of k_n^{∞} (see Section 3.4). Thus, we can compute the evolution of (σ_n,σ_m), for each cohesive surface, as plasticity develops during the loading. Such plots are reported in Fig. 6(b) for a point located at the crack tip, $x/r_t=0$, and another point in the bulk, at $x/r_t=0.4$. During loading, three domains can be distinguished in both stress trajectories in $\sigma_n-\sigma_m$ space: (i) an initial increase followed by (ii) a decrease and (iii) a final re-increase. These stages can be immediately linked to the constitutive response of the continuum reported in Fig. 1. We can identify qualitatively that (i) the initial increase in (σ_n,σ_m) coincides with the initial linear response, (ii) the subsequent decrease is related to the material softening while (iii) the final re-increase corresponds to the orientational hardening. The turning point in the (σ_n,σ_m) trajectory thus corresponds to the local yielding of the material.

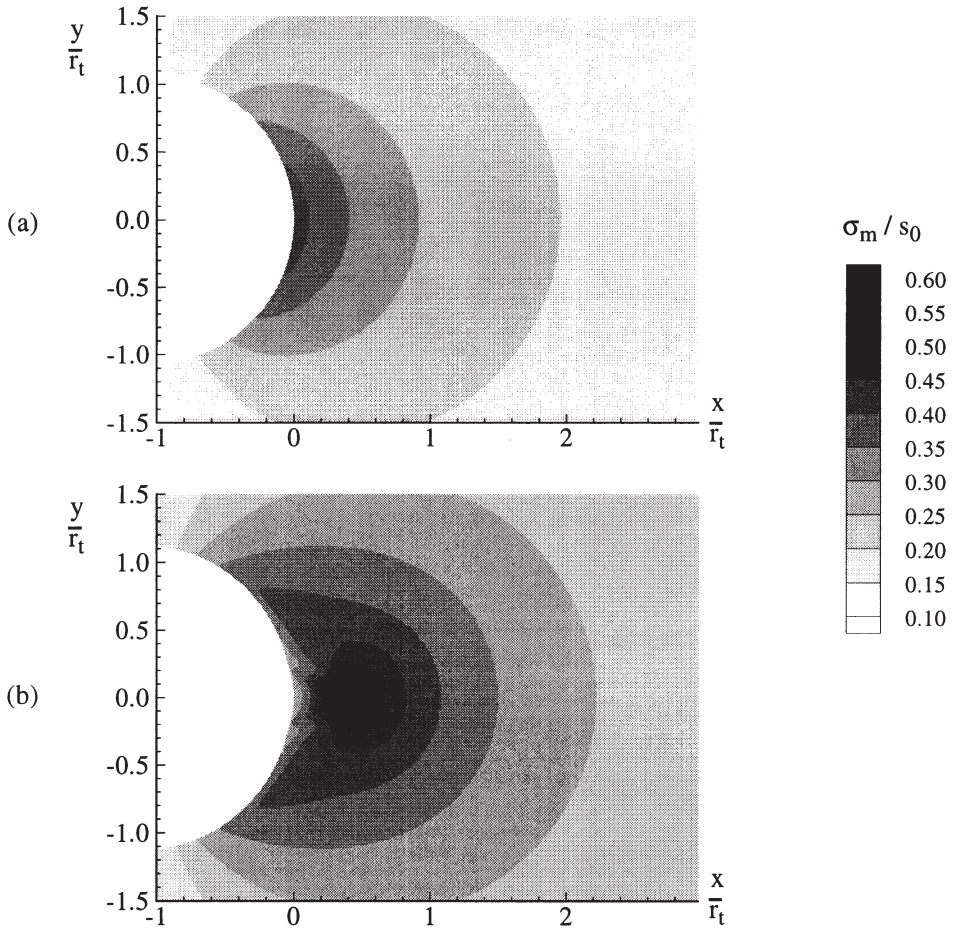

Fig. 7. Hydrostatic stress distribution, normalized by s_0, at craze initiation for craze parameters of (a) case 1 and (b) case 2.

The difference in trajectories for $x/r_t=0.4$ compared to that at $x/r_t=0$ is partly due to the development of plasticity around the crack tip as investigated in (Lai and Van der Giessen, 1997). Firstly, the hydrostatic stress generated at $x/r_t=0.4$ due to the plastic constraint tends to lower the slope of the first domain of the trajectory. Secondly, yield does not occur until a higher σ_n because of the hydrostatic stress dependency of $\dot{\gamma}^p$ according to Section 2.

Now, if a craze could be initiated, this last feature has a direct implication on the location of craze initiation. Crazing initiates whenever the local stress trajectory in $\sigma_n-\sigma_m$ space intercepts the craze initiation locus. For case number 1, this first occurs at the crack tip; the corresponding (σ_n,σ_m) at both locations are indicated in Fig. 6 by circles. For the second case, the crazing condition is not fulfilled at the crack tip when yielding of the material occurs, and subsequently the stress path turns. In this case, craze initiation first takes place for the cohesive surface located at $x/r_t=0.4$ (indicated by squares in Fig. 6). In both cases, craze initiation would take place in the region of highest hydrostatic stress as shown in Fig. 7(a) and (b).

Fig. 8 now shows the crack resistance curves[2] according to the coupled viscoplastic-crazing computation. The appearance of these two *R*-curves is typical of what is observed in all cases analyzed. After craze initiation and while the craze widens, the material response is ductile in the sense that further crazing requires an increase of the applied loading. However, as soon as fibrils start to break down, this rapidly propagates and unstable crack propagation takes place. In Figs. 9 and 10, we report the plastic shear rate distribution at different values of the loading as indicated in Fig. 8. These plots show the regions where plastic flow is taking place instantaneously. In these and subsequent figures, the value of $\dot{\gamma}^p$ is normalized by $\dot{\Gamma}_0=\dot{K}_I/(s_0\sqrt{r_t})$. At crazing initiation for case number 1, no significant plasticity is observed (not shown).

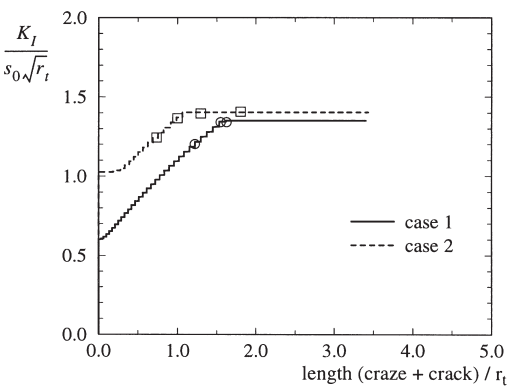

Fig. 8. Influence of the craze initiation parameters on the *R*-curves: (a) parameters of case 1, initiation at the crack tip, (b) parameters of case 2, initiation in the bulk.

[2] Crack resistance curve and R-curve refer to the plot of the stress intensity factor vs the crack and craze length.

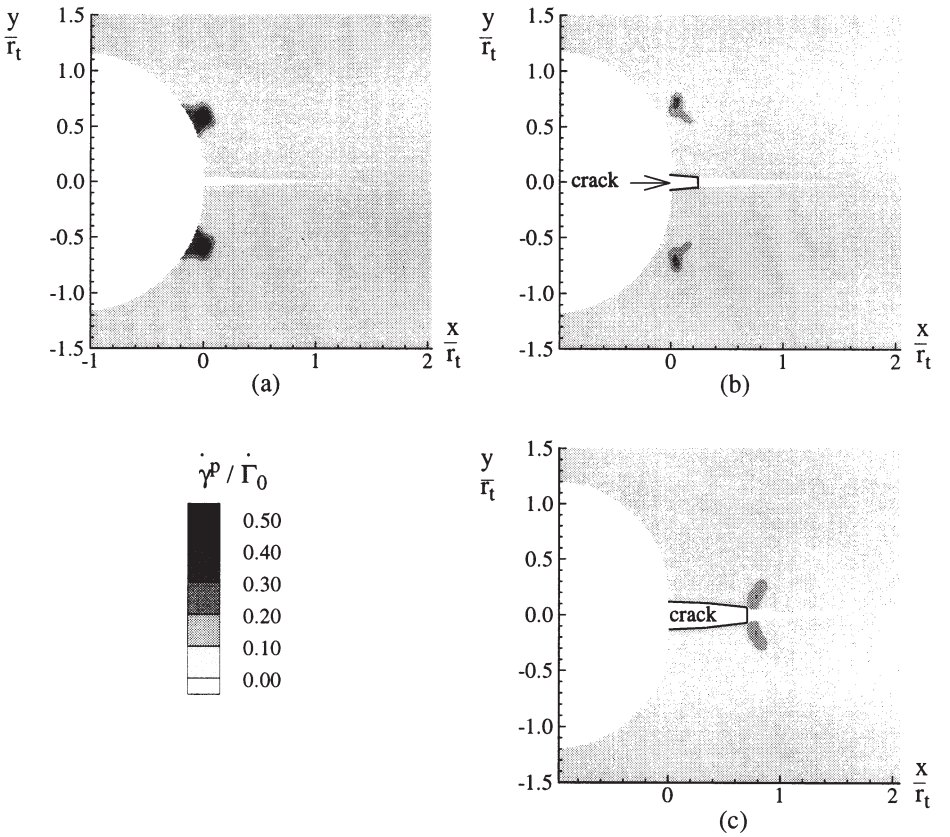

Fig. 9. Instantaneous plastic deformation for the craze parameter of case 1: (a) before craze fibrils break down, (b) and (c) during crack propagation.

For a higher B^0 (case number 2), yielding of the material is confined to a region closer to the crack tip and crazing initiates in the bulk. In both cases, we observe that plasticity develops until craze fibrils break down (Figs. 9(a) and 10(b)). Before fibrils breakdown, the hydrostatic stress distribution indicates the location of new craze initiation during the loading because of its implication in the initiation criterion.

In Fig. 11(a), we observe that maximum of this distribution is located at the craze tip, but that there are also two peaks beside the crack symmetry plane. The latter coincide with the location of major plasticity seen in Fig. 9(a). This suggest that crazing would not need to be restricted to the symmetry plane but may be more diffuse around the crack tip region. For the second set, the maximum hydrostatic stress before craze breakdown (see Fig. 11(b)) is located at the right craze tip, thus indicating the direction of further craze initiation. In this case, the first fibril breakdown coincides with the initiation location (x/r_t=0.4). Then, the crack propagates backwards to the original notch tip as indicated by the higher plastic strain-rate distribution at the left craze tip in Fig. 10(c). When the ligament between the internal

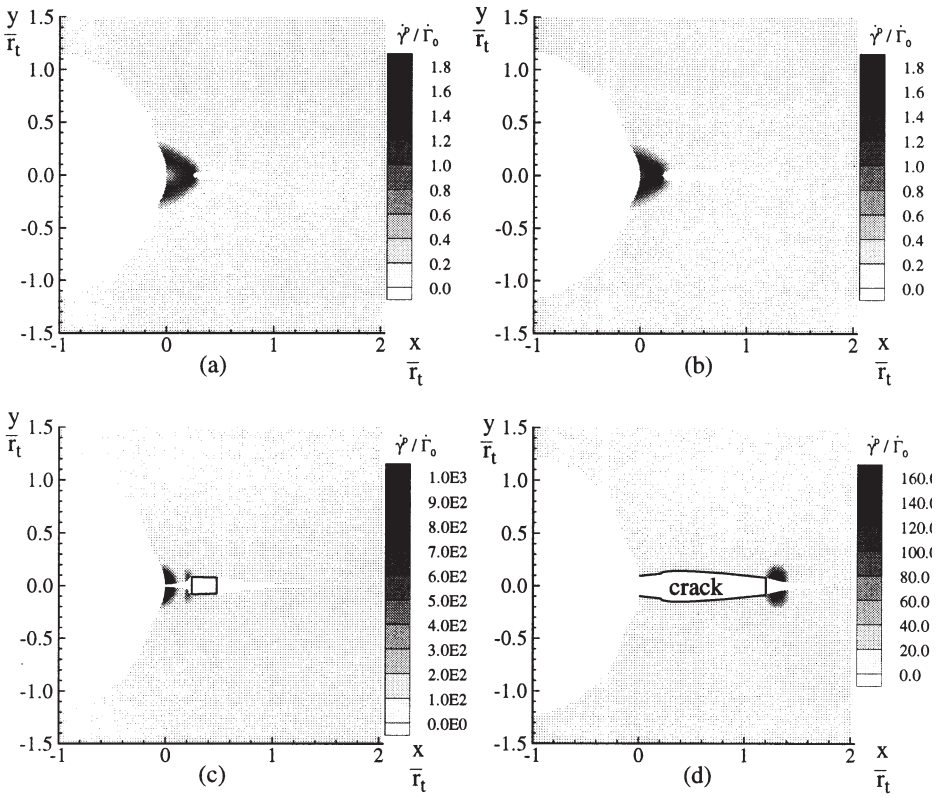

Fig. 10. Instantaneous plastic deformation for the craze parameter of case 2: (a) before craze initiation, (b) before craze fibrils break down, (c) and (d) during crack propagation.

crack and the initial crack has failed, crack propagation continues from the right-hand craze tip (see Fig. 10(d)) and is then similar to that observed in the reference case.

5.2. Influence of $\Delta_n^{c\,cr}$

According to Section 3.3, $\Delta_n^{c\,cr}$ is the material parameter which governs fibril breakdown and subsequent crack propagation. Because its effect is common to all the sets of parameters, we choose to illustrate it by using a smaller and a larger value of this parameter (cases number 3 and 4 in Table 2) when compared to the reference set (case number 1). The highest value of case number 4 is close to the upper limit to what can be used in our analysis since $\Delta_n^{c\,cr}/r_t=0.2$ leads to $\Delta_n^{c\,cr}=20\mu m$ for a crack tip radius of $r_t=0.1$ mm. Indeed, we indicated in the problem formulation that the material density within the craze is neglected by assuming that the bulk material density is not affected by the crazing. A larger value of $\Delta_n^{c\,cr}$ would lead to a craze width that is comparable to the crack tip radius. This would violate the applicability of a cohesive surface framework.

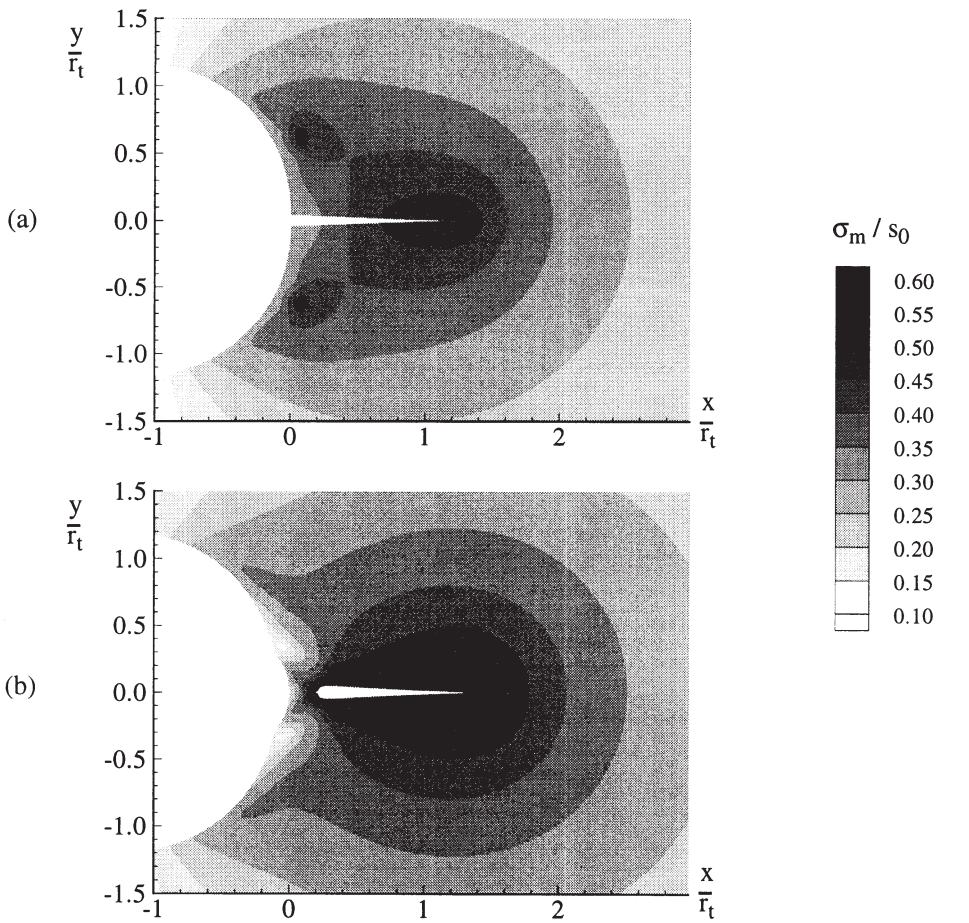

Fig. 11. Hydrostatic stress distribution just prior to craze fibril first breakdown for parameters of (a) case 1 and (b) case 2.

In Fig. 12, we report the R-curves corresponding to these three values of $\Delta_n^{c\,cr}$ (cases 1 (reference), 3 and 4). As $\Delta_n^{c\,cr}$ governs the instant of crack growth, an increase of $\Delta_n^{c\,cr}$ leads to crack propagation to occur for a higher loading level. This correlation would be linear if the response of the bulk polymer were purely elastic. In the present cases, the differences in K_I for unstable crack growth are altered by the increase of plasticity and related energy dissipation as $\Delta_n^{c\,cr}$ increases (see Fig. 13).

In Fig. 13(a)–(c), we present the plastic shear-rate distribution of each case (3, 1, 4, respectively) just prior to fibril breakdown. As long as the fibrils have not broken down, load is transmitted across the craze surfaces through the craze fibrils and plasticity can develop in the surrounding. The plastic development ceases when craze breakdown occurs. Then, the crack propagation by further fibrils breakdown and

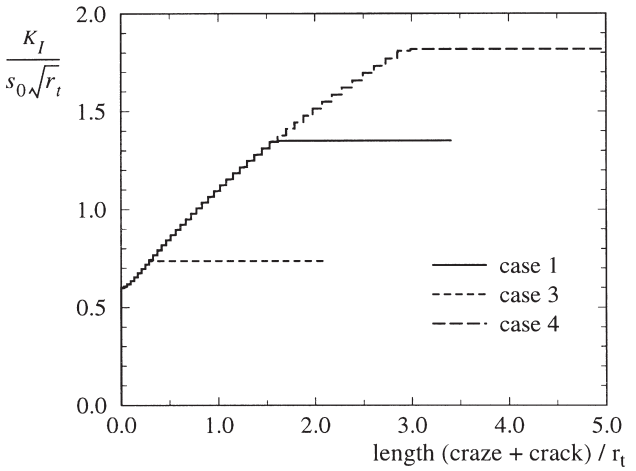

Fig. 12. Influence of $\Delta_n^{c\,cr}$ on the *R*-curves for the craze parameters of (a) case 1, $\Delta_n^{c\,cr}/r_t$=0.1, (b) case 3, $\Delta_n^{c\,cr}/r_t$=0.01, (c) case 4, $\Delta_n^{c\,cr}/r_t$=0.2.

related crack opening carries all the deformation so that the bulk response is largely elastic.

5.3. *Influence of the loading rate* $\dot{K}_I$

The results presented in the first two subsections were obtained for a loading rate of $\dot{K}_I \equiv \dot{K}_I^0 \approx 3\times10^{-2}MPa\sqrt{\text{m}}$/sec. We here investigate the influence of loading rate for the reference craze parameters (case number 1 in Table 2) by using two other loading rates of $\dot{K}_I \approx 30\dot{K}_I^0$ and $900\dot{K}_I^0$. Each of the *R*-curves for the three loading rates, shown in Fig. 14, have the same characteristics as those discussed previously. A noticeable feature of these curves, however, is that when $\dot{K}_I$ increases, the critical K_I^{cr} also increases. Moreover the critical length of the craze (when $K_I=K_I^{cr}$) decreases when the loading rate increases (note that no crack propagation has taken place before K_I^{cr} is reached).

Within the standard framework of fracture mechanics, this dependence of K_I^{cr} on the applied loading rate is quite surprising. Indeed, when the loading rate increases, it implies less viscoplastic activity in the bulk material (see Fig. 13(b) for the lowest loading rate, the two others cases are not reported since the material plasticity is almost negligible) and consequently less energy dissipated by plastic deformation. Then from a straightforward Griffith argument, the required applied K_I^{cr} for crack propagation would be expected to decrease with increasing loading rate. On the other hand, if one uses a critical COD argument, one could argue that the toughness would increase with loading rate in the case of a viscoelastic material. Nevertheless, it should be realized that in the case of glassy polymers, crack propagation is preceded by crazing and crack formation is related to the breakdown of fibrils. Even in the absence of plastic deformation in the bulk, crazing itself implies a time scale for

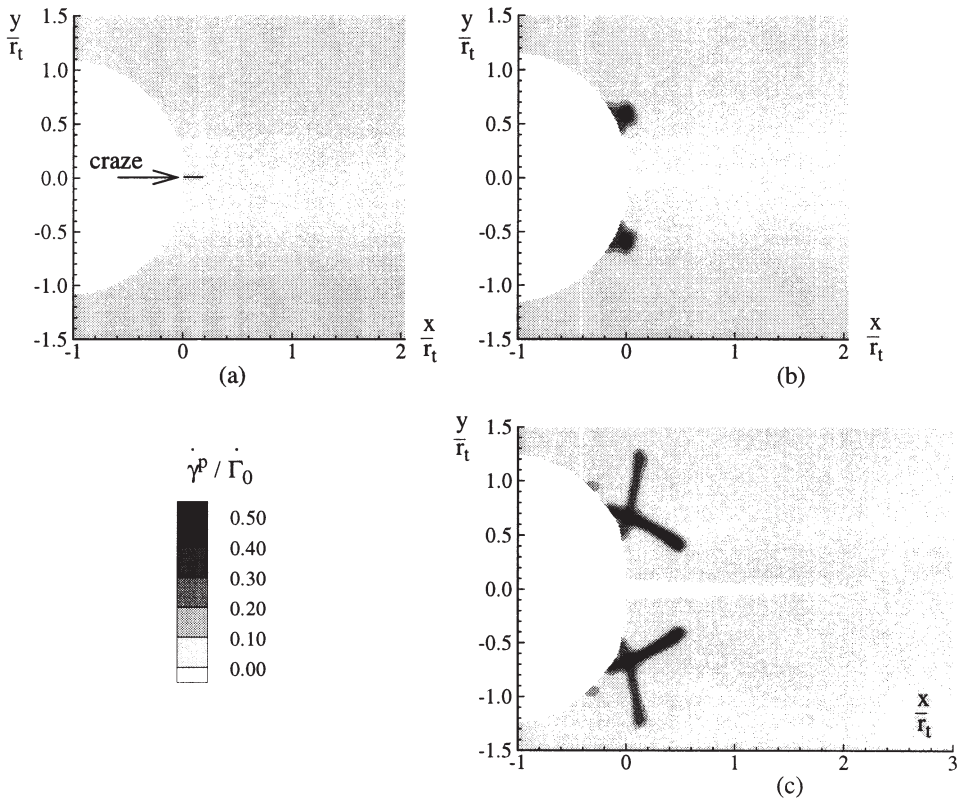

Fig. 13. Influence of $\Delta_n^{c\,cr}$ on the instantaneous plastic flow distribution before craze breakdown for craze parameters of (a) case 1, $\Delta_n^{c\,cr}/r_t$=0.1, (b) case 3, $\Delta_n^{c\,cr}/r_t$=0.01, (c) case 4, $\Delta_n^{c\,cr}/r_t$=0.2.

reaching the fibril breakdown condition $\Delta_n^c=\Delta_n^{c\,cr}$ since craze widening is a viscoplastic process. A standard approach for brittle fracture by defining a critical energy stored for crack propagation cannot be invoked therefore.

In our problem, to get an insight of the effect of the loading rate, we need to distinguish three time scales introduced by (i) the loading rate $\dot{K}_I$; (ii) the reference shear rate $\dot{\gamma}^0$ in the bulk viscoplasticity, Eq. (4); and (iii) the $\dot{\Delta}^0$ appearing in Eq. (12) and represent the crazing time dependency. This set implies two independent ratios. For the reference craze parameters (case number 1), an increase of the loading rate is equivalent to a decrease of the bulk viscoplasticity for a given applied loading, because the ratio $\dot{K}_I/\dot{\gamma}^0$ also increases. Hence, it becomes immediately clear that the material response tends to be less viscoplastic, yielding a reduced development of hydrostatic stress due to the viscoplastic constraint. Since the hydrostatic stress is key in the craze initiation (Eqs. (10) and (11)), its decrease tends to delay craze initiation. Furthermore, the ratio $\dot{K}_I/\dot{\Delta}^0$ increases when the loading rate increases; this is equivalent to a reduced craze widening activity for the same applied loading rate. Therefore, craze breakdown is delayed in time, thus leading to a higher K_I^{cr}.

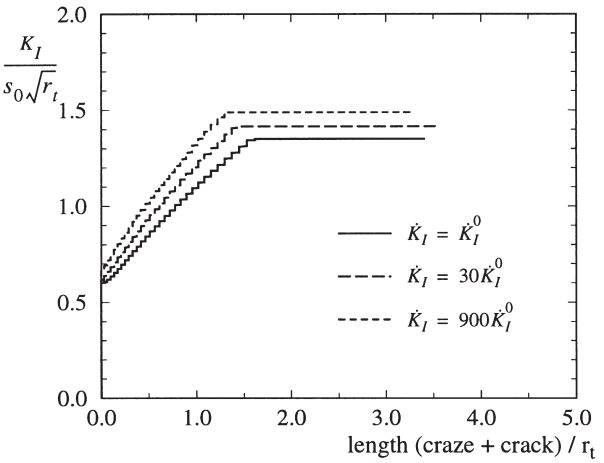

Fig. 14. Influence of the loading rate $\dot{K}_I$ on the *R*-curves using the craze parameters of case 1 for $\dot{K}_I$=: (a) $\dot{K}_I^0$, (b) $30\dot{K}_I^0$, (c) $900\dot{K}_I^0$.

When no significant viscoplasticity is observed in the bulk material, the kinetics of craze widening appears as the key feature for the critical stress intensity factor for the material. Therefore, in the last two subsections, we investigate the effect of the parameters involved in the craze widening relation Eq. (12): Δ_0 and A^c.

5.4. Influence of $\dot{\Delta}_0$

In the previous subsections, the parameters in the reference set (case number 1 in Table 2) are such that no significant viscoplastic deformation in the bulk is observed when unstable crack propagation takes place (see Fig. 13(a) and (b)) except when a large value of the critical craze width is considered (case number 4 reported in Fig. 13(c)). In the previous subsection, we have pointed out the importance of the ratios $\dot{K}_I/\dot{\gamma}^0$, $\dot{K}_I/\dot{\Delta}^0$ in interpreting the results and also $\dot{\gamma}^0/\dot{\Delta}^0$ is required. We here vary the reference widening rate $\dot{\Delta}^0$ in Eq. (12) by considering cases 5, 6 and 7 in Table 2 in which its value is reduced each time by a factor of ten relative to the value for case 1. A decrease of $\dot{\Delta}^0$ leads to an increase of $\dot{K}_I/\dot{\Delta}^0$ and $\dot{\gamma}^0/\dot{\Delta}^0$ so that for a given applied loading, the craze widening rate decreases. The condition of fibril breakdown at $\Delta_n^c=\Delta_n^{c\,cr}$ is then delayed in time while the bulk material viscoplasticity is enhanced as indicated by the increase in $\dot{\gamma}^0/\dot{\Delta}^0$. The loading rate is kept at the reference value of $\dot{K}_I=\dot{K}_I^0$.

The corresponding resistance curves are reported in Fig. 15 while the plastic strain rate distribution before fibril breakdown is shown in Fig. 16(a)–(d) for cases 1, 5–7, respectively. From Fig. 15, we observe that a first reduction of the parameter $\dot{\Delta}_0$ leads to a significantly higher K_I^{cr}. This is related to a higher viscoplasticity in the bulk, as indicated in Fig. 16(b), compared to the reference case (Fig. 16(a)). By comparing the results for the cases 5, 6 and 7, however, we find that once noticeable viscoplastic development takes place, K_I^{cr} varies slightly with further $\dot{\Delta}^0$ reduction.

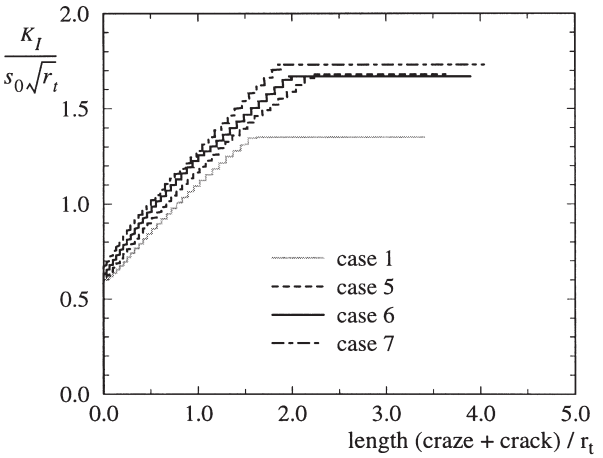

Fig. 15. Influence of $\dot{\Delta}^0$ on the *R*-curves for the craze parameters of (a) case 1, $\dot{\Delta}^0/r_t$=100 s^{-1}, (b) case 5, $\dot{\Delta}^0/r_t$=10 s^{-1}, (c) case 6, $\dot{\Delta}^0/r_t$=1 s^{-1}, (d) case 7, $\dot{\Delta}^0/r_t$=0.1 s^{-1}.

An interesting feature of these latter results is that, while the craze still initiates at the crack tip, fibril breakdown starts at the intersection of shear bands (in the material bulk) where significant plastic deformation occurs (Fig. 16(b)–(d)). Incidentally, it is important in interpreting these results to realize that Fig. 16 reports the instantaneous viscoplastic activity. In Fig. 16(d), the plastic strain rate distribution appears lower than that in Fig. 16(c), because deformation in the bulk involves significant orientational hardening. Nevertheless, the accumulated plastic strain is higher, as indicated by a larger plastic zone in Fig. 16(d) when compared to that in Fig. 16(c).

The variations of $\dot{\Delta}_0$ performed in this subsection indicate that two regimes can be distinguished: (i) for sufficiently large $\dot{\Delta}_0$ (compared to $\dot{K}_I$ and $\dot{\gamma}^p$), unstable failure of the material occurs without noticeable viscoplasticity when fibrils break down; (ii) for sufficiently low $\dot{\Delta}_0$ the material has undergone large plasticity around the crack tip when unstable crack propagation takes place, and craze fibril breakdown coincides with the shear band intersections. In the latter case, plastic flow provides a significant accommodation mechanism for craze widening.

It is finally worth noting that the maximum variation in $\dot{K}_I/\dot{\Delta}^0$ by a factor of 1000 is roughly the same as that considered in Section 5.3 by varying the loading rate by a factor of 900 at constant $\dot{\Delta}_0$. In both cases, increasing this ratio leads to an increase in K_I^{cr}; this increase is about 10% when the loading rate varies (see Fig. 14) and roughly 25% when the craze kinetics are modified (see Fig. 15). In the first case, increasing $\dot{K}_I/\dot{\Delta}^0$ leads to a lower craze widening rate so that the condition $\Delta_n^c=\Delta_n^{c\,cr}$ is delayed in time and therefore K_I^{cr} increases. In the second case, the ratio $\dot{\gamma}^p/\dot{\Delta}^0$ increases as well, and therefore K_I^{cr} is further increased due to energy dissipation by plastic deformation in the bulk prior to craze fibril breakdown.

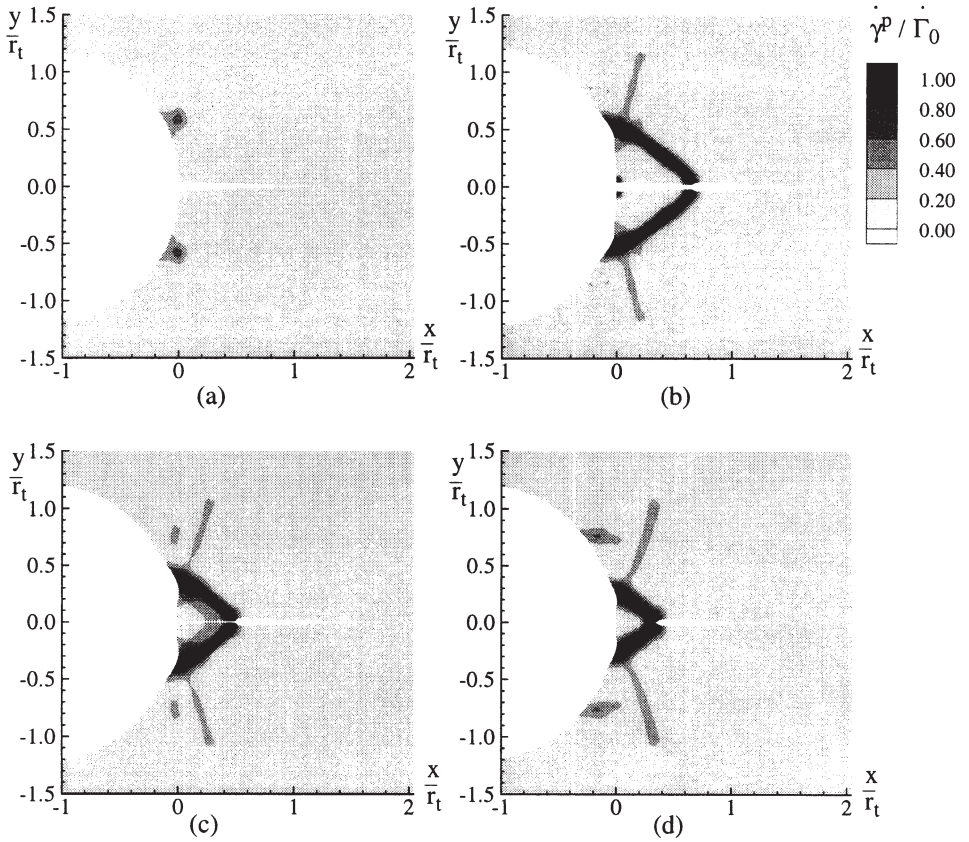

Fig. 16. Influence of $\dot{\Delta}_0$ on the instantaneous plastic flow distribution before craze breakdown for craze parameters of (a) case 1, $\dot{\Delta}^0/r_t$=100 s^{-1}, (b) case 5, $\dot{\Delta}^0/r_t$=10 s^{-1}, (c) case 6, $\dot{\Delta}^0/r_t$=1 s^{-1}, (d) case 7, $\dot{\Delta}^0/r_t$=0.1 s^{-1}.

5.5. *Influence of craze temperature dependence A^c*

The parameter A^c in Eq. (12) for the craze opening rate controls the temperature dependence of the stress necessary for craze widening. When Eq. (12) is rewritten as

$$\frac{\sigma_n}{\sigma^c}=\frac{T}{A^c\sigma^c}\ln\left(\frac{\dot{\Delta}_n^c}{\dot{\Delta}^0}\right)+1, \tag{23}$$

it is immediately clear that the stress necessary for a given widening rate $\dot{\Delta}_n^c/\dot{\Delta}^0(<1)$ decreases linearly with temperature, as determined by $T/A^c\sigma^c$. The computations discussed above have used a value of A^c equal to that of A in Eq. (4), which implies a similar temperature dependency for the craze widening rate and the bulk plastic strain rate. We here explore the influence of A^c versus A by comparing the numerical predictions obtained by using the reference craze parameters (case number 1) and

those of case number 8 where A^c is three times larger. We re-investigate the effect of the loading rate $\dot{K}_I$ by using those used in Section 5.3 ($\dot{K}_I^0 30\dot{K}_I^0$ and $900\dot{K}_I^0$) and also an intermediate value of $120\dot{K}_I^0$.

For each loading rate, the *R*-curves corresponding to the case number 8 are reported in Fig. 17. We observe that the critical stress intensity factor as well as the critical length of the craze decrease when the loading rate increases. The corresponding plots of the plastic strain rate, just before craze fibril breakdown, are reported in Fig. 18(a)–(d).

In these figures, three types of responses can be distinguished: (i) for the loading rates $\dot{K}_I^0$ and $30\dot{K}_I^0$, a rather large plastic zone had developed before crack growth; (ii) for $\dot{K}_I=120\dot{K}_I^0$, an intermediate situation arises in which shear bands initiate but plasticity reduces due to crazing; (iii) the deformation of the bulk is largely elastic for $\dot{K}_I=900\dot{K}_I^0$. For the two lowest loading rates ($\dot{K}_I^0$ and $30\dot{K}_I^0$), crazing initiates at the crack tip, but craze breakdown takes place at the shear bands intersection (see Fig. 18(a) and (b)). For the two highest loading rates ($120\dot{K}_I^0$ and $900\dot{K}_I^0$), craze initiation and breakdown coincide, and take place at the crack tip. In cases 1 and 8, the effect of the loading rate on the bulk viscoplasticity is identical, since the ratio $\dot{K}_I/\dot{\gamma}^p$ in the two cases is the same.

Hence, the results in Figs. 14 and 17 indicate that the effect of the loading rate depends to a large extent on the competition between plasticity and crazing through the change of $\dot{\gamma}^p/\dot{\Delta}_n^c$. An increase of $\dot{K}_I$ leads to an increase of $\dot{K}_I/\dot{\gamma}^p$ and $\dot{K}_I/\dot{\Delta}_n^c$, which is equivalent to a decrease of $\dot{\gamma}^p$ and $\dot{\Delta}_n^c$ at constant $\dot{K}_I$. For a given stress state, such a decrease in $\dot{\gamma}^p$ and $\dot{\Delta}_n^c$ corresponds to a temperature decrease according to Eqs. (4) and (12). As in this study, the temperature dependence of the crazing is lower than that of the bulk plasticity ($A^c>A$), the ratio $\dot{\gamma}^p/\dot{\Delta}_n^c$ diminishes as the loading rate increases. This effect is revealed by a decreasing plasticity of the bulk at fibril break-

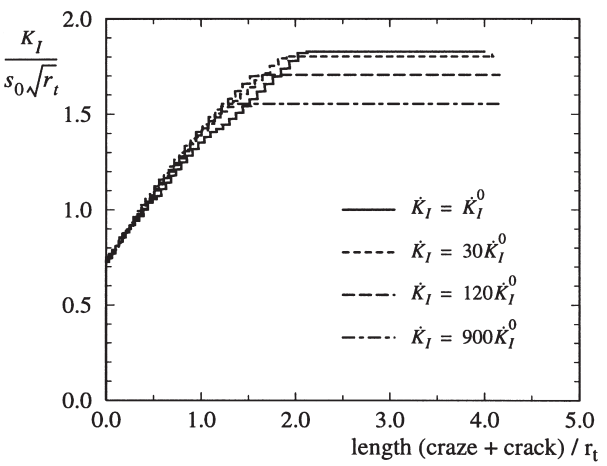

Fig. 17. Influence of the craze parameter A^c on the *R*-curves using the craze parameters of case 8 for $\dot{K}_I$=: (a)$\dot{K}_I^0$, (b) $30\dot{K}_I^0$, (c) $120\dot{K}_I^0$, (d) $900\dot{K}_I^0$.

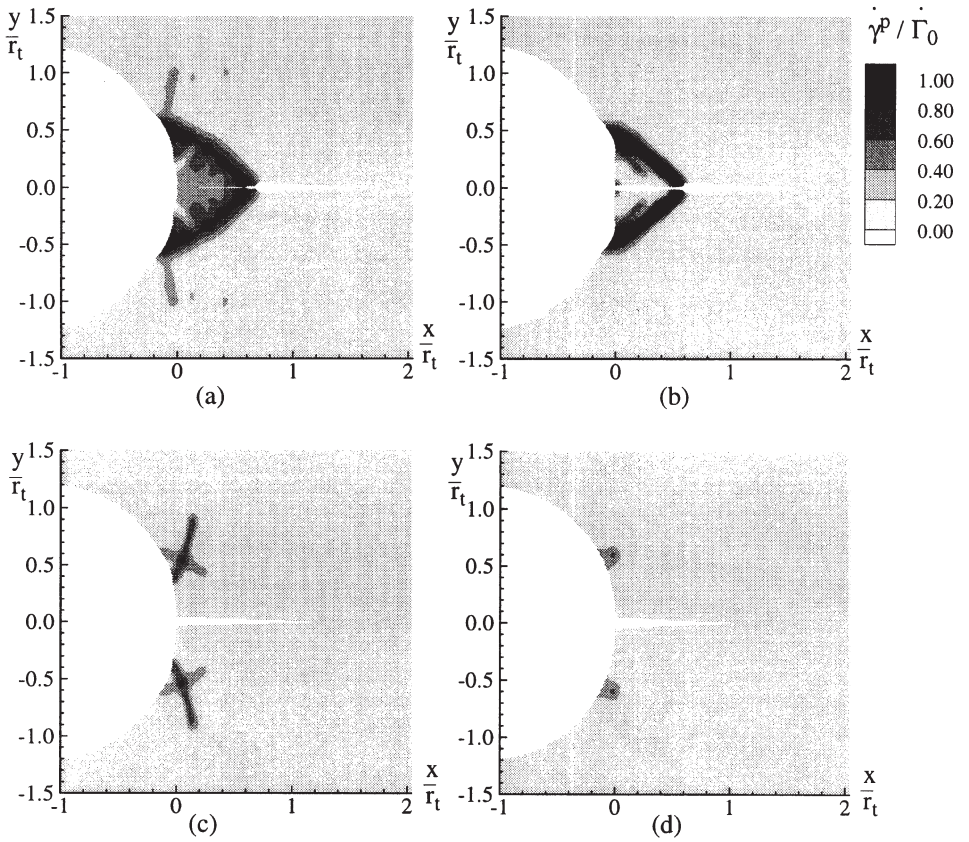

Fig. 18. Influence of the craze parameter A^c on the instantaneous plastic flow distribution before craze fibrils breakdown using the craze parameters of case 8 for $\dot{K}_I$=: (a) $\dot{K}_I^0$, (b) $30\dot{K}_I^0$, (c) $120\dot{K}_I^0$, (d) $900\dot{K}_I^0$.

down as $\dot{K}_I$ increases (see Fig. 18). For case number 8, for $\dot{K}_I$=$900\dot{K}_I^0$, the deformation of the bulk is mainly elastic (Fig. 18) and $K_I^{cr}/(s_0\sqrt{r_t})\approx 1.5$ (Fig. 17(d)) and very close to that of the reference case for the same loading rate condition (Fig. 14).

6. Conclusion

We have investigated the initial stages of crack propagation from an initially blunt notch in an amorphous glassy polymer. The analysis accounts for viscoplastic flow in the bulk which typically leads to initiation and propagation of shear bands. Fracture occurs through crazing, which is incorporated through a cohesive surface model. The material model includes stress-dependent craze initiation, rate-dependent craze widening and a critical craze opening for breakdown. A parameter study has been carried out to investigate the competition between viscoplasticity and crazing in controlling the fracture toughness.

Craze initiation criterion depends on A^0, B^0 and the mean stress distribution (Section 3.1), of which the maximum location coincides with that of crazing initiation. At small critical openings of the craze, for instance case number 3 with $\Delta_n^{c\,cr}/r_t$=0.01 (see Fig. 12), a slight difference between the value of K_I at initiation and K_I^{cr} is predicted. In such conditions, the stress state at craze initiation is close to that of unstable crack propagation and governs the failure of the material.

As $\Delta_n^{c\,cr}$ increases, craze initiation cannot be simply considered as a precursor to brittle failure according to the difference of K_I at craze initiation and K_I^{cr} (see Fig. 12). Then, plastic deformation around the initial notch and around the craze front dissipate energy, thus leading to an increased fracture toughness of the material. The actual toughness is found to depend on the competition between plasticity and crazing, as characterized by the ratio $\dot{\gamma}^p/\dot{\Delta}_n^c$ at some appropriate location. From the point of view of material properties, this ratio is primarily controlled by the ratio $\dot{\gamma}_0/\dot{\Delta}^0$ between the time scale of plastic flow and craze widening. In case of a variable loading rate, $\dot{K}_I$, this introduces another time scale, so that the ratios $\dot{K}_I/\dot{\Delta}^0$ and/or $\dot{K}_I/\dot{\gamma}_0$ also control the competition. The fracture toughness for unstable crack propagation is the outcome of this competition; it generally is not a material parameter.

The competition between plasticity and crazing is particularly important before breakdown of the craze fibrils starts. As pointed out in Section 5.5, the influence on the critical value of K_I for unstable crack propagation is determined by the amount of viscoplastic deformation that has developed during the time span between craze initiation to craze breakdown. The onset of fibril breakdown practically coincides with unstable crack propagation for the range of parameters considered here.

The interaction between plasticity and crazing also determines the location at which breakdown of the mature craze occurs and the crack starts to grow. When crazing is dominant, the location of craze breakdown coincides with that of craze initiation. This can be either at the tip of the notch or in the bulk at the intersection of shear bands. When substantial plastic deformation has developed during craze widening, craze fibril breakdown tends to start where the associated shear bands intersect; this location can be different from that of craze initiation. Indeed, Ishikawa and Ogawa (1981) observed mature crazes ahead of a notch in polycarbonate at the intersection of shear bands, but it is not clear whether the craze actually initiated there or only grew to become visible there.

From the present numerical results, it is to be expected that the crack growth velocity in amorphous polymers is also controlled by the kinetics of both local plastic deformation and crazing. This velocity is typically measured at constant load and such experiments often show that the crack growth velocity increases with the applied stress intensity. The present computations cannot be used to confront the model with such experiments. This will be the subject of future work.

References

Argon, A.S., 1973. A theory for the low-temperature plastic deformation of glassy polymers. Phil. Mag. 28, 839–865.

Argon, A.S., Hannoosh, J.G., 1977. Initiation of crazes in polystyrene. Phil. Mag. 36 (5), 1195–1216.
Argon, A.S., Salama, M.M., 1977. Growth of crazes in glassy polymers. Phil. Mag. 36 (5), 1217–1234.
Arruda, E.M., Boyce, M.C., 1993. A three-dimensional constitutive model for large stretch behaviour of rubber elastic materials. J. Mech. Phys. Solids 41 (2), 389–412.
Berger, L.L., 1990. On the mechanism of craze fibril breakdown in glassy polymers. Macromolecules 23, 2926–2934.
Berger, L.L., Sauer, B.B., 1991. Enhanced segmental mobility at polymer surfaces: thermally stimulated current studies of crazed films. Macromolecules 24, 2096–2099.
Boyce, M.C., Parks, D.M., Argon, A.S., 1988. Large inelastic deformation of glassy polymers. Part I: rate dependent constitutive model. Mech. Mater. 7, 15–33.
Brown, H.R., Kramer, E.J., 1981. Craze microstructure from small-angle X-ray scattering (SAXS). J. Macromol. Sci.-Phys. B19 (3), 487–522.
Bucknall, C.B., 1977. Toughened Plastics. Applied Science Publications, London.
Döll, W., 1983. Optical interference measurements and fracture mechanics analysis of crack tip craze zones. Adv. Polym. Sc. 52, 105–168.
Döll, W., Könczöl, L., 1990. Micromechanics of fracture: optical interferometry of crack tip craze zone. Adv. Polym. Sc. 91, 138–214.
Donald, A.M., Kramer, E.J., 1981. The mechanism of craze-tip advance in glassy polymers. Phil. Mag. A 43 (4), 857–870.
Donald, A.M., Kramer, E.J., 1982. The entanglement network and craze micromechanics in glassy polymers. J. Polymer Sci. 20, 1129–1141.
Haward, R.N., 1973. The Physics of Glassy Polymers. Applied Science Publishers, London.
Hui, C.Y., Ruina, A., Creton, C., Kramer, E.J., 1992. Micromechanics of crack growth into a craze in a polymer glass. Macromolecules 25, 3948–3955.
Ishikawa, M., Ogawa, H., 1981. Brittle fracture in glassy polymers. J. Macromol. Sci.-Phys. B19 (3), 421–443.
Ishikawa, M., Takahashi, H., 1991. Crazing mechanism based on plastic instability. J. Mat. Sci. 26, 1295–1300.
Ishikawa, M., Narisawa, I., Ogawa, H., 1977. Criterion for craze nucleation in polycarbonate. J. of Polym. Sci. 15, 1791–1804.
Kambour, R.P., 1973. A review of crazing and fracture in thermoplastics. J. Polym. Sci., Macromolecular Reviews 7, 1–154.
Kinloch, A.J., Young, R.J., 1983. Fracture Behaviour of Polymers. Elsevier Applied Science, London.
Kramer, H.H., 1983. Microscopic and molecular fundamentals of crazing. Adv. Polym. Sc. 52, 1–56.
Kramer, H.H., Berger, L.L., 1990. Craze growth and fracture. Adv. Polym. Sc. 91, 1–68.
Lai, J., Van der Giessen, E., 1997. A numerical study of crack-tip plasticity in glassy polymers. Mech. Mater. 25, 183–197.
Lauterwasser, B.D., Kramer, E.J., 1979. Microscopic mechanisms and mechanics of craze growth and fracture. Phil. Mag. A 39 (4), 469–495.
Needleman, A., 1987. A continuum model for void nucleation by inclusion debonding. J. Appl. Mech. 54, 525–531.
Sha, Y., Hui, C.Y., Ruina, A., Kramer, E.J., 1997. Detailed simulation of craze fibril failure at a crack tip in a glassy polymer. Acta Mater. 45, 3555–3563.
Sternstein, S.S., Myers, F.A., 1973. Yielding of glassy polymers in the second quadrant of principal stress space. J. Macromol. Sci.-Phys. B 8 (3/4), 539–571.
Sternstein, S.S., Ongchin, L., 1969. Yield criteria for plastic deformation of glassy high polymers in general stress fields. Polymer preprints 10 (2), 1117–1124.
Tijssens, M.G.A., Van der Giessen, E., Sluys, L.J., 2000. Modeling of crazing using a cohesive surface methodology. Mech. Mat. 32, 19–35.
Van der Giessen, E., Lai, J., 1997. Deformation, Yield and Fracture of Polymers, vol. 10. The Institute of Materials, London, pp. 35–38.
Van der Giessen, E., 1997. Localized plastic deformations in glassy polymers. Eur. J. Mech. A/Solids 16, 87–106.

Wu, P.D., Van der Giessen, E., 1993. On improved network models for rubber elasticity and their applications to orientation hardening in glassy polymers. J. Mech. Phys. Solids 41 (3), 427–456.
Wu, P.D., Van der Giessen, E., 1996. Computational aspects of localized deformations in amorphous glassy polymers. Eur. J. Mech. A/Solids 15 (5), 799–823.
Williams, J.G., 1984. Fracture Mechanics of Polymers. Ellis Horwood.